Applied Catalysis B: Environmental 92 (2009) 437–444

Contents lists available at ScienceDirect

Applied Catalysis B: Environmental

journal homepage: www.elsevier.com/locate/apcatb

Effect of large cations (La^{3+} and Ba^{2+}) on the catalytic performance of Mn-substituted hexaaluminates for N_2O decomposition

Ming Tian [a,b], Aiqin Wang [a], Xiaodong Wang [a,*], Yanyan Zhu [a,b], Tao Zhang [a,**]

[a] State Key Laboratory of Catalysis, Dalian Institute of Chemical Physics, Chinese Academy of Sciences, Dalian 116023, PR China
[b] Graduate University of Chinese Academy of Sciences, Beijing 100049, PR China

ARTICLE INFO

Article history:
Received 17 July 2009
Received in revised form 25 August 2009
Accepted 2 September 2009
Available online 12 September 2009

Keywords:
N_2O decomposition
Propellant
Manganese
Hexaaluminate

ABSTRACT

Mn-substituted La-hexaaluminate ($LaMn_xAl_{(12-x)}O_{19}$) and Ba-hexaaluminate ($BaMn_xAl_{(12-x)}O_{19}$) catalysts were prepared using the carbonates route and investigated for high-concentration of N_2O decomposition. It was for the first time found that the Ba-hexaaluminate exhibited higher activity than the La-hexaaluminate at a given Mn content, both of which were much more active than Mn/Al_2O_3 after being subjected to high-temperature (1400 °C) treatment. The catalytic activity varied with the Mn content and attained the best one at $x = 1$. X-ray diffraction (XRD) characterizations showed that a small amount of Mn (up to $x = 1$) promoted greatly the formation of phase-pure hexaaluminate, while excess Mn caused formation of catalytically inactive impurity phases, such as $LaAlO_3$, $BaAl_2O_4$, Mn_3O_4, and $LaMnO_3$, which covered partially the active sites and then led to a loss of the activity. UV–visible spectra showed that Mn^{2+} preferentially enter tetrahedral Al sites at a low Mn content ($x = 0.5$) for the La-hexaaluminate, which is quite different from the case of Ba-hexaaluminate where Mn^{3+} can substitute octahedral Al sites even at $x = 0.5$. Such a difference in the number of catalytically active Mn^{3+} sites in the octahedral position should be responsible for the higher activity of the Mn-substituted Ba-hexaaluminate.

© 2009 Elsevier B.V. All rights reserved.

1. Introduction

N_2O is being considered as a promising green propellant used for small satellite propulsion systems due to its low toxicity compared with traditional hydrazine propellant, as well as its capability for self-pressurizing and compatibility with the common construction materials [1,2]. The chemistry for N_2O as a propellant lies in that the decomposition of N_2O into N_2 and O_2 accompanies with a large amount of heat release and volume expansion, which can be used as propulsion power. Quite different from the abatement of environmental pollutant N_2O where the concentration of N_2O is only in ppm level [3–6], the N_2O used as the propellant must have a high-concentration, even being a pure chemical, so as to generate the propulsion power as high as possible. However, the decomposition of pure N_2O is a highly exothermic reaction (the enthalpy is −82 kJ/mol) and leads to a temperature rise over 1000 °C [1,2,7]. In this case, the catalysts used for N_2O propellant must have a very good thermal stability. Actually, the high-temperature stability of a material has become a paramount factor to be considered for evaluating its feasibility as the catalyst for N_2O propellant.

Hexaaluminates are a class of excellent high-temperature materials thanks to their unique peculiar layered structure consisting of γ-Al_2O_3 spinel blocks intercalated by mirror planes in which the large cations (Ba, Ca, La and Sr) are locating [8–11]. More importantly, the aluminium cations in the spinel blocks can be substituted with transition metals, giving rise to redox centers for a variety of catalytic reactions [12,13]. In our previous work [14,15], via introduction of Ir into the Fe-substituted $BaAl_{11}O_{19}$ hexaaluminate we obtained a novel catalyst for N_2O propellant decomposition which can initiate the reaction at a low temperature (350 °C) and can maintain the stable performance at a temperature as high as 1200 °C. Nevertheless, the loss of the active component Ir is still inevitable, in particular after many cycles of startup-shutdown. A possible solution to this problem is to develop a two-bed reactor, in which the Ir-hexaaluminate or other more active catalyst constitutes the front bed while the back bed requires a more thermally stable catalyst, just like the dual-bed in CH_4 combustion [16,17]. To this end, we investigated the Mn-substituted hexaaluminates for the catalytic decomposition of high-concentration of N_2O in the present work, with a focus on the effect of large cations (Ba^{2+} and La^{3+}).

Mn-substituted hexaaluminates have been regarded as the most active catalysts for methane combustion reaction [18–23].

* Corresponding author. Tel.: +86 411 84379680; fax: +86 411 84685940.
** Corresponding author. Tel.: +86 411 84379015; fax: +86 411 84691570.
E-mail addresses: xdwang@dicp.ac.cn (X. Wang), taozhang@dicp.ac.cn (T. Zhang).

0926-3373/$ – see front matter © 2009 Elsevier B.V. All rights reserved.
doi:10.1016/j.apcatb.2009.09.002

Various studies have been devoted to the effect of large cations (La^{3+}, Ba^{2+}, Sr^{2+}, Mg^{2+}) on the performance of the Mn-substituted hexaaluminates for the catalytic combustion of methane. The size of different cations (the radius of La^{3+}, Ba^{2+} and Sr^{2+} is 1.06 Å, 1.35 Å and 1.12 Å, respectively) may influence the structure of hexaaluminate, and then the oxidation state of Mn species. Jang et al. reported that $LaMn_1Al_{11}O_{19}$ was much more active than the $BaMn_1Al_{11}O_{19}$, and they ascribed the activity enhancement to the different oxidation state of Mn ions in the two types of hexaaluminates [24]. Partial substitution of La^{3+} with Sr^{2+} ($Sr_{1-x}La_xMnAl_{11}O_{19}$) could further enhance [25] or diminish [26] the catalytic activity of the Mn-substituted hexaaluminates, while incorporation of Mg^{2+} into the $LaMn_1Al_{11}O_{19}$ largely increased the catalytic activity by stabilizing the Mn ions at a high oxidation state [27]. Li and Wang prepared Mn-substituted Ba-La-hexaaluminate rod-like nanoparticles and found that $Ba_{0.2}La_{0.8}MnAl_{11}O_{19}$ catalyst exhibited much higher activity than either $BaMnAl_{11}O_{19}$ or $LaMnAl_{11}O_{19}$ [28]. Evidently, the nature of large cations in the Mn-substituted hexaaluminates affect significantly the Mn^{2+}/Mn^{3+} redox cycle, and then the catalytic performance. However, the influences of large cations have rarely been investigated for N_2O decomposition. Recently, Pérez-Ramírez et al. investigated a series of metal-substituted hexaaluminates $ABAl_{11}O_{19}$ (A = La, Ba, and B = Mn, Fe, Ni) for high-temperature N_2O abatement [29,30]. They claimed that both Fe- and Mn-substituted hexaaluminates were active for this reaction, but the influence of large cations were not investigated in detail. In the present work we found that Ba-hexaaluminate was much more active than the La-hexaaluminate at the fixed Mn content. In order to gain an insight into the effect of large cations, a variety of characterization techniques were employed to reveal the relationship between structure and oxidation state of Mn cations in the two types of hexaaluminates. Finally, a two-bed reactor was designed to evaluate the feasibility for pure N_2O propellant decomposition in a thruster.

2. Experimental

2.1. Catalyst preparation

La-Mn-Al oxide catalysts ($LaMnAl_{11}O_{19}$, denoted as LMA-t, t indicates calcination temperature) and Ba-Mn-Al oxide catalysts ($BaMnAl_{11}O_{19}$, denoted as BMA-t) were prepared by coprecipitation with $(NH_4)_2CO_3$. For example, to prepare LMA-t, 1.08 g of $La(NO_3)_3{\cdot}6H_2O$, 0.90 g of $Mn(NO_3)_2$ (50%), and 10.31 g of $Al(NO_3)_3{\cdot}9H_2O$ were dissolved individually in deionized water at 60 °C, and then added into a saturated aqueous solution of $(NH_4)_2CO_3$ under stirring to form the hexaaluminate precursor precipitate. After continuous stirring at 60 °C for 3 h, the precipitate was filtered, washed with deionized water, and then dried at 120 °C overnight. Finally, the sample was calcined in air at 500 °C, 800 °C, 1000 °C, 1200 °C, and 1400 °C for 4 h, to obtain LMA-500, LMA-800, LMA-1000, LMA-1200, and LMA-1400, respectively. Similarly, the BMA-t samples were prepared by the above procedure except $Ba(NO_3)_2$ as the barium salt precursor. For comparison, Mn/Al_2O_3 was also prepared by the above coprecipitation procedure with $Al(NO_3)_3{\cdot}9H_2O$ and Mn $(NO_3)_2$ (50%) as the starting materials.

To study the effect of Mn content in the hexaaluminates, $LaMn_xAl_{(12-x)}O_{19}$-1200 and $BaMn_xAl_{(12-x)}O_{19}$-1200 catalysts with different Mn content (x = 0, 0.5, 1, 2, and 3) were also prepared by the above-described procedure just by varying the amount of $Mn(NO_3)_2$ and $Al(NO_3)_3{\cdot}9H_2O$ added.

To investigate the reproducibility of the above preparation method, three batches of BMA-1200 samples were prepared. Both the XRD characterizations and the activity tests for N_2O decomposition showed the identical results in an accepted error range, demonstrating good reproducibility of this method.

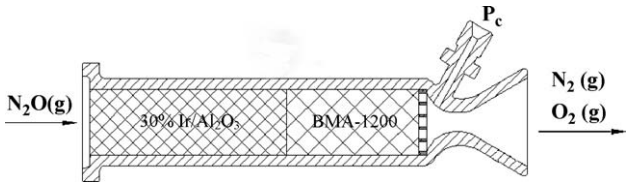

Fig. 1. Schematic illustration of two-bed catalyst configuration in a 0.1 N thruster.

2.2. Catalytic activity measurements

The activity measurements were conducted in a fixed-bed flow reaction system as described previously [15]. Prior to the reaction, the catalyst was pretreated in Ar at 300 °C for 0.5 h. Then, the reaction gas containing 30 vol.% N_2O in Ar passed through 100 mg of the catalyst sample at a flow rate of 50 mL/min (STP), corresponding to a gas hour space velocity (GHSV) of 30,000 mL/h g. The bed temperature was increased from 450 °C to 800 °C at an increment of 50 °C, and held at each temperature for 25 min to reach a steady state. The effluent gas was on-line analyzed by Agilent 6890N gas chromatograph equipped with Chromosorb 103 column and Molecular Sieve 13X column. N_2O conversion was calculated from the difference between the inlet and outlet concentrations.

The feasibility of the Mn-substituted hexaaluminate as the bulk-bed catalyst for N_2O propellant decomposition was evaluated with a 0.1 N microthruster (30 mm long, 6 mm diameter). As illustrated in Fig. 1, the front bed (18 mm long) of the microthruster was loaded with 30%Ir/Al_2O_3 catalyst [31,32] while the back bed (12 mm long) was BMA-1200 catalyst. All the catalysts were pelletized into grains of 20–40 meshes. Pure N_2O gas was provided by saturated pressure of liquid N_2O at 20 °C and 5.2 MPa, and was injected into the microthruster with a flow rate of 2.8 L/min. Before ignition, the catalyst bed was preheated to a specified temperature. The chamber pressure (P_c) was plotted against the reaction time.

2.3. Characterization

The metal contents of the samples were determined by inductively coupled plasma (ICP) and X-ray fluorescence (XRF). The Brunauer–Emmett–Teller (BET) specific surface areas were measured by nitrogen adsorption at −196 °C on a Micromeritics ASAP 2010 apparatus. The X-ray diffraction (XRD) patterns were recorded with a PANalytical X'Pert-Pro powder X-ray diffractormeter, using Cu Kα monochromatized radiation (λ = 0.1541 nm) at a scan speed of 5°/min. Scanning electron microscopy (SEM) experiments were performed with a JSM 6360-LV electron microscope operating at 20–25 kV. The samples were vapor-deposited with gold before analysis. UV–visible spectra were obtained on a Cintra (GBC) apparatus with $BaSO_4$ as a reference.

3. Results and discussion

3.1. Effect of calcination temperature on the phase composition and catalytic performance

Fig. 2 shows the XRD patterns of LMA-t and BMA-t samples which were obtained by calcination of precursors at different temperatures. For comparison, Mn/Al_2O_3-t samples were also characterized by XRD. In agreement with the results in literature [27], 500 °C-calcination of the precursors only results in amorphous structure, regardless of large cations (Ba^{2+} or La^{3+}). In contrast, intense XRD peaks corresponding to Mn_2O_3 [JCPDS No. 89-4836] are clearly observed together with the broad peaks of

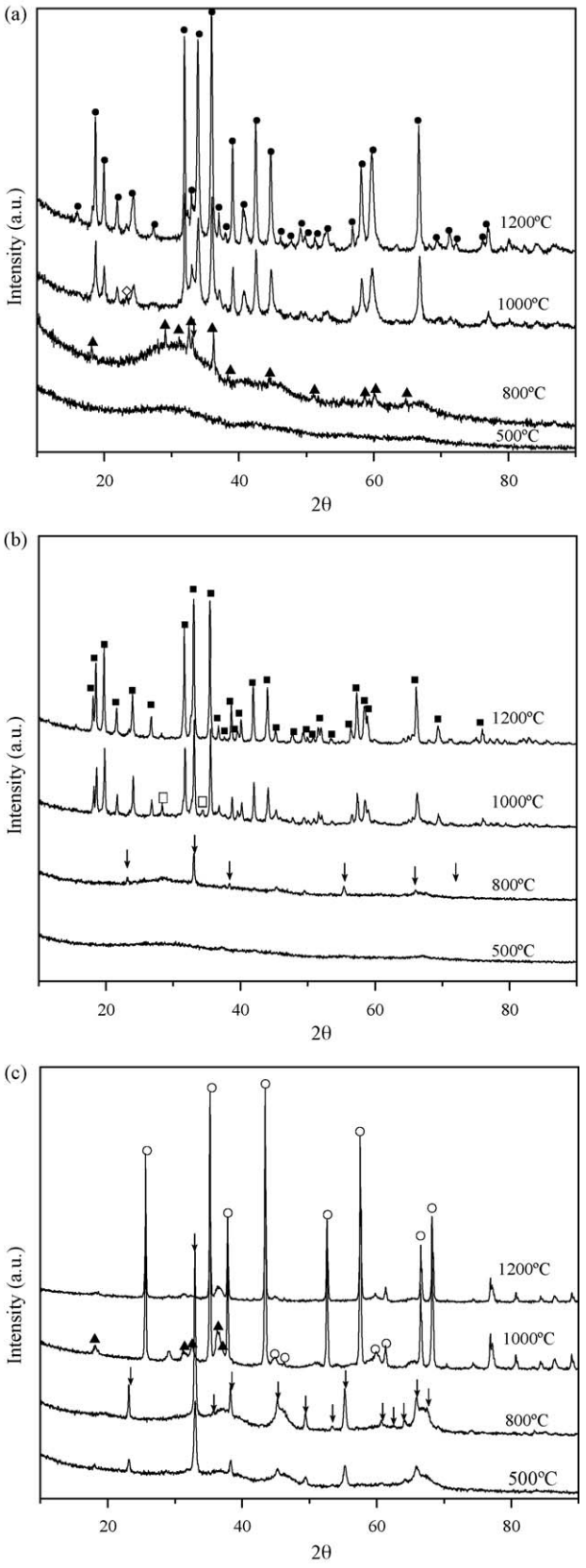

Fig. 2. X-ray diffraction patterns of (a) LMA-t and (b) BMA-t and (c) Mn/Al_2O_3-t catalysts. (↓) Mn_2O_3, (▲) Mn_3O_4, (●) $LaAl_{11}O_{18}$, (◇) $LaAlO_3$, (■) $BaAl_{12}O_{19}$, (□) $BaAl_2O_4$, (○) α-Al_2O_3.

γ-Al_2O_3 for Mn/Al_2O_3 sample. This result suggests that either La^{3+} or Ba^{2+} can promote greatly the homogeneous dispersion of Mn and Al oxides. When the calcination temperature was elevated to 800 °C, the Mn_2O_3 peaks of the Mn/Al_2O_3 sample became stronger but no additional peaks appear. The same XRD peaks corresponding to Mn_2O_3 appear also on the BMA-800 sample but their intensities are very low. On the other hand, the LMA-800 presents only Mn_3O_4 phase [JCPDS No. 1-1127]. Obviously, the type of large cations strongly affects the oxidation state of Mn ions. For both the LMA and BMA samples, further increasing the calcination temperature to 1000 °C led to the formation of hexaaluminates. Meanwhile, the XRD peaks of the Mn oxides disappear completely and some new peaks corresponding to $LaAlO_3$ (for the LMA sample) or $BaAl_2O_4$ (for the BMA sample) appear at this temperature. In contrast to the LMA and BMA samples, the Mn/Al_2O_3-1000 presents rather sharp diffraction peaks of α-Al_2O_3. At the same time, the original Mn_2O_3 phase was transformed into Mn_3O_4 for the latter phase is more thermodynamically stable [33]. Upon raising the calcination temperature to 1200 °C, monophasic hexaaluminates were produced for both the LMA and the BMA samples, whereas the α-Al_2O_3 peaks on the Mn/Al_2O_3 became sharper due to sintering of particles. It is noted that the intensities of Mn_3O_4 diffraction peaks on the Mn/Al_2O_3 have a large decrease at 1200 °C. Examinations of the Mn contents of this sample revealed approximately 50% of the original Mn content was lost during the high-temperature calcinations, which is in contrast with the almost constant Mn content in the LMA and BMA samples. This result unambiguously indicates the stabilization of Mn species by the peculiar layered structure of hexaaluminates. Compared with our previous reported Ir-substituted hexaaluminate [14,15], the Mn-substituted hexaaluminates have much better stabilities which makes them promising candidates as a back-bed catalyst for N_2O propellant decomposition.

Table 1 lists the BET surface areas of LMA-t, BMA-t, and Mn/Al_2O_3-t samples. For clarity, the phase compositions at each calcination temperature are also summarized in Table 1. As expected, the BET surface areas of the three types of catalysts decrease continuously with increasing the calcination temperature. In particular, significant loss of the surface areas took place when the samples were calcined at 1000 °C. As described above, phase transformation starts at this temperature, i.e., amorphous structure is transformed into hexaaluminates for both the LMA and BMA samples while metastable Mn_2O_3 and γ-Al_2O_3 are transformed respectively into thermally stable Mn_3O_4 and α-Al_2O_3. Significant sintering occurs accompanied with phase transformations, which results in a great loss in specific surface areas. It must be stressed that both the LMA-1200 and BMA-1200 present much larger surface areas than the Mn/Al_2O_3-1200 does, demonstrating the outstanding sintering-resistant property of the hexaaluminates. The SEM images in Fig. 3 clearly show the small aggregates particles of the LMA-1200 and BMA-1200 in contrast with the

Table 1
BET surface area and phase composition for LMA-t, BMA-t and Mn/Al_2O_3-t.

Catalysts	BET surface area (m^2/g)	Phase composition
LMA-500	123	Amorphous
LMA-800	106	Amorphous + Mn_3O_4
LMA-1000	33	$LaAl_{11}O_{18}$, $LaAlO_3$
LMA-1200	27	$LaAl_{11}O_{18}$
BMA-500	117	Amorphous
BMA-800	86	Amorphous + Mn_2O_3
BMA-1000	40	$BaAl_{12}O_{19}$, $BaAl_2O_4$
BMA-1200	21	$BaAl_{12}O_{19}$
Mn/Al_2O_3-500	246	Mn_2O_3
Mn/Al_2O_3-800	152	Mn_2O_3
Mn/Al_2O_3-1000	17	Mn_3O_4, α-Al_2O_3
Mn/Al_2O_3-1200	7	Mn_3O_4, α-Al_2O_3

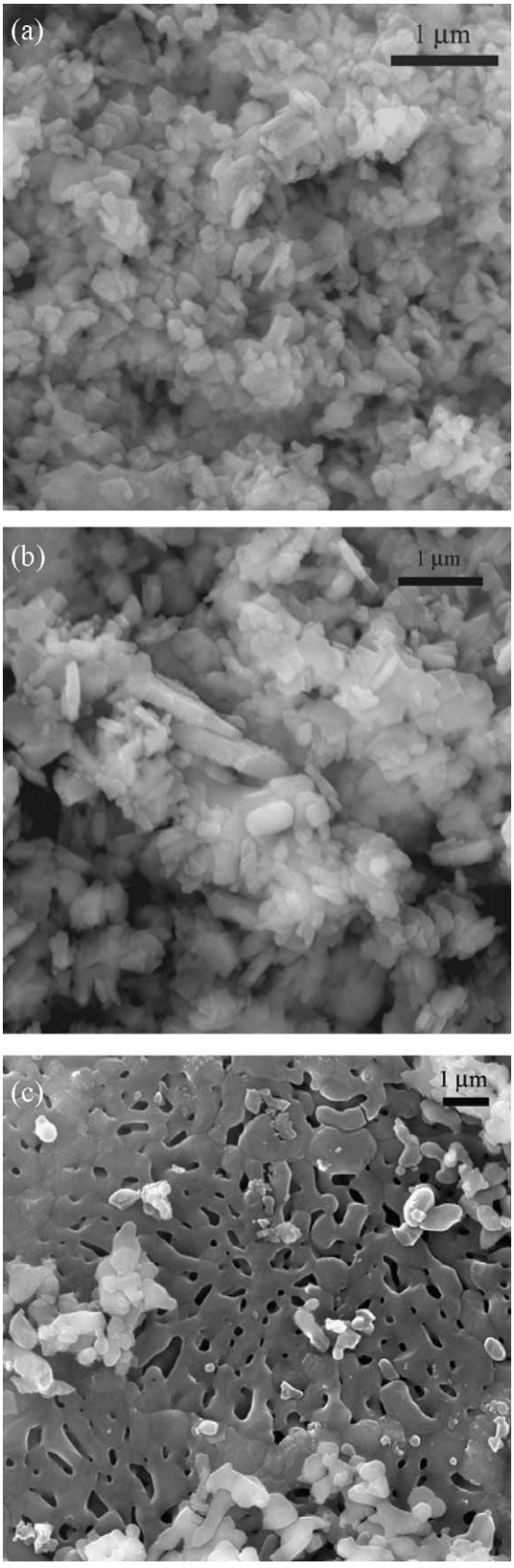

Fig. 3. Scanning electron micrographs of (a) LMA-1200, (b) BMA-1200 and (c) Mn/Al_2O_3-1200.

extensive sintering of the Mn/Al_2O_3-1200 particles, which should be attributed to the peculiar layered structure of the hexaaluminates [34,35].

The catalytic performances of the LMA-t and BMA-t samples were evaluated for 30 vol.% N_2O decomposition. Fig. 4 depicts the profiles of N_2O conversion versus the reaction temperature over the two types of catalysts. For both the LMA-t and BMA-t catalysts, the activities increased with the calcination temperature up to the highest at 1200 °C, except for the lowest activity of the samples calcined at 800 °C. Considering the phase compositions and surface areas at different calcination temperatures (Table 1), one can see that the Mn species in the hexaaluminates are much more active than that in the amorphous structure although the latter has larger surface area. Moreover, the BMA-1200 exhibited higher activity than the LMA-1200. For example, the N_2O conversion at 650 °C over the BMA-1200 attained above 90% while it was only 67% over the LMA-1200. In contrast with the Mn-substituted hexaaluminates, the activities of the Mn/Al_2O_3-t catalysts decreased monotonically with increasing the calcination temperature, in line with the change of specific surface areas. It is noted that the Mn/Al_2O_3-500 exhibited even higher activity than the LMA-1200, suggesting that the Mn_2O_3 species in the Mn/Al_2O_3-500 catalyst is the active phase for N_2O decomposition. Unfortunately, the Mn/Al_2O_3 cannot resist the high temperature, which excludes the possibility of its application in high-temperature reactions, such as CH_4 combustion [36–38] and pure N_2O decomposition [1,14,39].

The stabilities of the catalysts were further investigated at 650 °C with the time-on-stream. As shown in Fig. 5, the N_2O conversion remains constant over 40 h time-on-stream for all the three catalysts, i.e., LMA-1200, BMA-1200, and Mn/Al_2O_3-1200, demonstrating excellent stabilities of the catalysts. However, the activity level differs greatly at this reaction temperature. The N_2O conversion over the BMA-1200 was the highest one, up to 92%, among the three catalysts. On the other hand, it was only 33% over the Mn/Al_2O_3-1200, indicating its poor activity due to significant sintering and volatilization of the active Mn species.

3.2. Effect of Mn content on the structure and catalytic performance of LMA and BMA

Since the Mn species incorporated into the hexaaluminates is the active component for N_2O decomposition, one would expect more Mn ions could enter into the structure of the hexaaluminate in order to further enhance the catalytic activity. Fig. 6 illustrates the XRD patterns of the $LaMn_xAl_{(12-x)}O_{19}$-1200 and $BaMn_xAl_{(12-x)}O_{19}$-1200 catalysts with different Mn content. In the absence of Mn ($x = 0$), diffraction peaks corresponding to $LaAlO_3$ and $BaAl_2O_4$ are clearly observed, together with the hexaaluminate phase. With an increase of the Mn content, the impurity $LaAlO_3$ and $BaAl_2O_4$ phases gradually decrease, and then almost disappear up to $x = 1$. This result is consistent with the previous report that transition metal ions (like Fe, Mn, Ni, etc.) significantly promoted the formation of hexalauminate [34,40]. Further increasing the Mn content brought about again the appearance of the impurity phases including $LaAlO_3$, $BaAl_2O_4$, $LaMnO_3$, and Mn_3O_4. Hence, the optimum content of Mn is at the x value equaling to 1, at which pure crystalline hexaaluminate can be obtained. According to literature [13,27], further prolonging the calcination time or elevating the calcination temperature promoted the formation of phase-pure hexaaluminate, even without Mn ion or containing more than one Mn ion. From the cell parameters listed in Table 2, one can see that the value of a_0 ($a_0 = b_0$) continuously increases with the Mn content in the hexaaluminates. However, when the x value increased from 2 to 3, the increment of a_0 is negligible, indicating that not all of the Mn cations can enter into the framework of hexaaluminate at a high Mn concentration. The

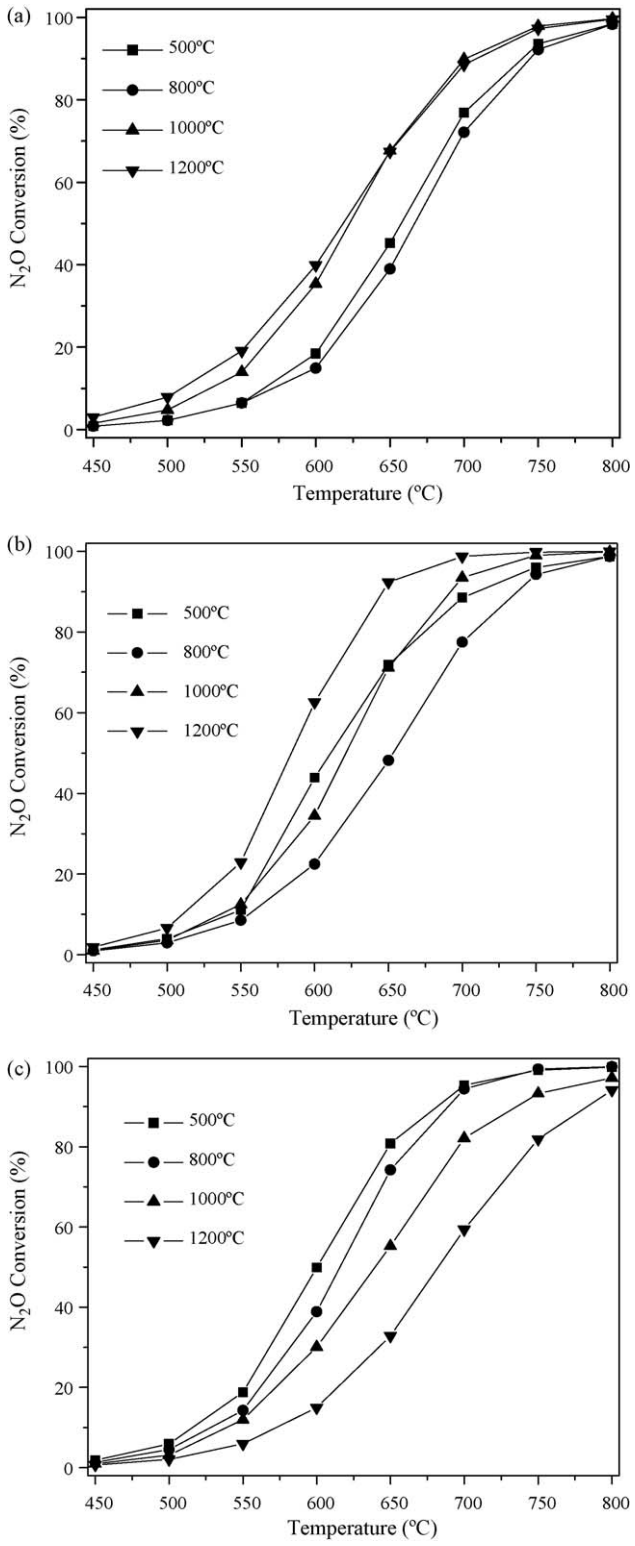

Fig. 4. Effect of calcination temperature on the catalytic performances of (a) LMA-t, (b) BMA-t and (c) Mn/Al_2O_3-t catalysts.

excess Mn cations exist as Mn_3O_4 in the case of Ba-hexaaluminate or as $LaMnO_3$ in the case of La-hexaaluminate, as evidenced by XRD results in Fig. 5. It is noted that the cell parameters of the $BaMn_xAl_{(12-x)}O_{19}$ are larger than those of $LaMn_xAl_{(12-x)}O_{19}$ due to bigger radius of Ba^{2+}.

Fig. 7 illustrates the N_2O conversions as a function of the reaction temperature over a series of $LaMn_xAl_{(12-x)}O_{19}$-1200 and

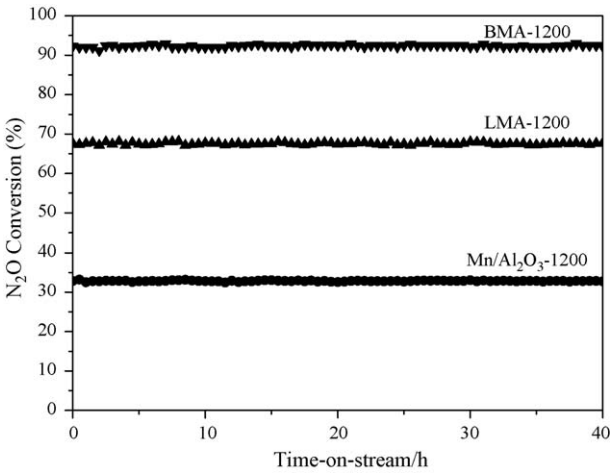

Fig. 5. N_2O conversion at 650 °C as a function of the time-on-stream over BMA-1200 (▼), LMA-1200 (▲) and Mn/Al_2O_3-1200 (●).

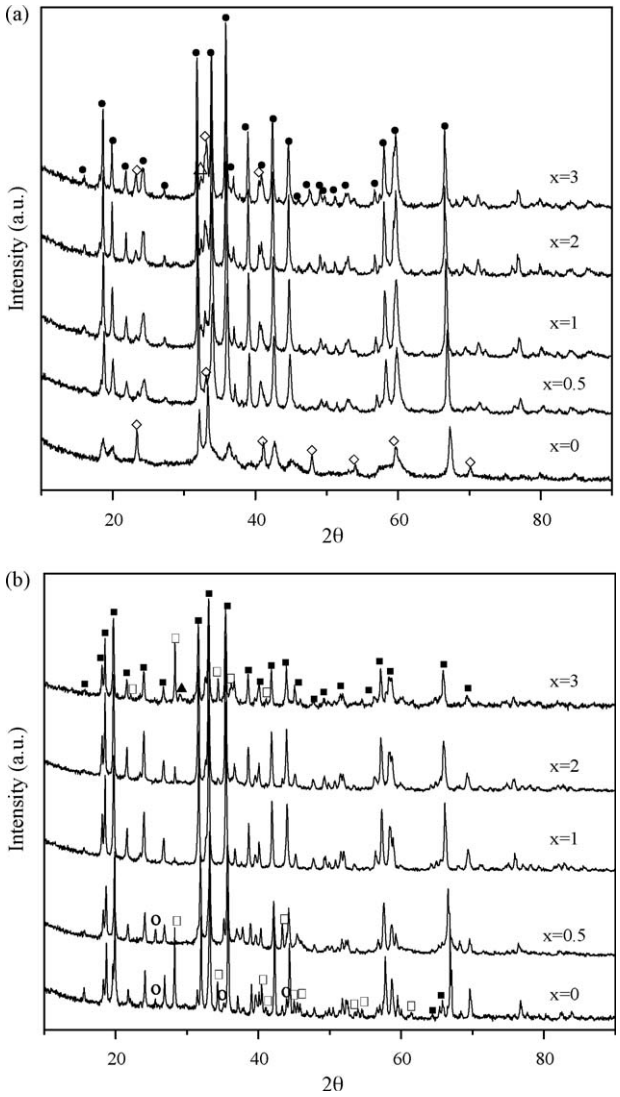

Fig. 6. X-ray diffraction patterns of (a) $LaMn_xAl_{(12-x)}O_{19}$-1200 and (b) $BaMn_xAl_{(12-x)}O_{19}$-1200 catalysts with different x values. (●) $LaAl_{11}O_{18}$, (◇) $LaAlO_3$, (■) $BaAl_{12}O_{19}$, (□) $BaAl_2O_4$, (○) α-Al_2O_3, (△) $LaMnO_3$, (▲) Mn_3O_4.

Table 2
Cell parameters of $LaMn_xAl_{(12-x)}O_{19}$-1200 and $BaMn_xAl_{(12-x)}O_{19}$-1200.

Catalysts		Cell parameters (Å)	Mn content (wt%)	
		$a_0 = b_0$	Theoretical amount	Actual amount
La	$x = 0$	5.576	0	0
	$x = 0.5$	5.582	3.5	2.4
	$x = 1$	5.598	6.9	5.3
	$x = 2$	5.612	13.4	10.9
	$x = 3$	5.617	19.4	17.8
Ba	$x = 0$	5.591	0	0
	$x = 0.5$	5.608	3.5	2.6
	$x = 1$	5.631	6.9	6.9
	$x = 2$	5.656	13.4	12.4
	$x = 3$	5.659	19.4	19.4

$BaMn_xAl_{(12-x)}O_{19}$-1200 catalysts with different Mn contents (x values). When $x = 0$, the $BaAl_{12}O_{19}$ hexaaluminate was only slightly active for N_2O decomposition, with the N_2O conversion of 47% at 800 °C. In comparison, the $LaAl_{12}O_{19}$-1200 was more active, over which the N_2O conversion arrived at 75% at 800 °C. Upon Mn incorporation, the catalytic activity had a large increase, especially for the Ba-hexaaluminate. A common feature for the two types of catalysts is that the catalytic activity increases with the Mn content, up to $x = 1$; then decreases with further increasing the Mn content. Clearly, there exists an optimum value of the Mn content ($x = 1$) for the Mn-substituted hexaaluminates in catalyzing the N_2O decomposition. From the XRD characterizations one can see that too much amount of Mn cations inevitably results in the formation of impurity phases, such as $LaAlO_3$, $BaAl_2O_4$, $LaMnO_3$, and Mn_3O_4. These catalytically inactive phases may cover the active sites of the hexaaluminates, leading to the loss of the activity. It is also noted that at a given x value, the $BaMn_xAl_{(12-x)}O_{19}$-1200 is always more active than the $LaMn_xAl_{(12-x)}O_{19}$-1200 catalyst, and their difference is particularly prominent at $x = 0.5$.

To uncover further the underlying reason for this activity difference, we performed the UV–vis characterizations. Fig. 8 shows diffuse reflectance UV–vis spectra of the $LaMn_xAl_{(12-x)}O_{19}$ and $BaMn_xAl_{(12-x)}O_{19}$ with different Mn contents. For the $LaMn_xAl_{(12-x)}O_{19}$ catalyst, when $x = 0.5$, four absorption bands can be observed at 225 nm, 255 nm, 425 nm, and 455 nm. According to literature [41,42], the band at 255 nm is associated with $O^{2-} \rightarrow Mn^{2+}$ charge transfer transition and the bands at 425 nm and 455 nm are attributed to Mn^{2+} ions in tetrahedral position. Thus, at a low Mn content, Mn preferentially replace the tetrahedral Al in the La-hexaaluminate structure with dominant oxidation state of 2+ [27]. When $x = 1$, the bands at 425 nm and 455 nm disappear and the two new broad bands appear at 490–510 nm and 690–710 nm, which can be assigned to Mn^{3+} in the distorted octahedral site [13,28,41,42]. It was reported that when Mn^{2+} and Mn^{3+} coexist in the sample, the absorption bands of Mn^{3+} will cover those of Mn^{2+} because the spin allowed Mn^{3+} d–d transitions are strong while the

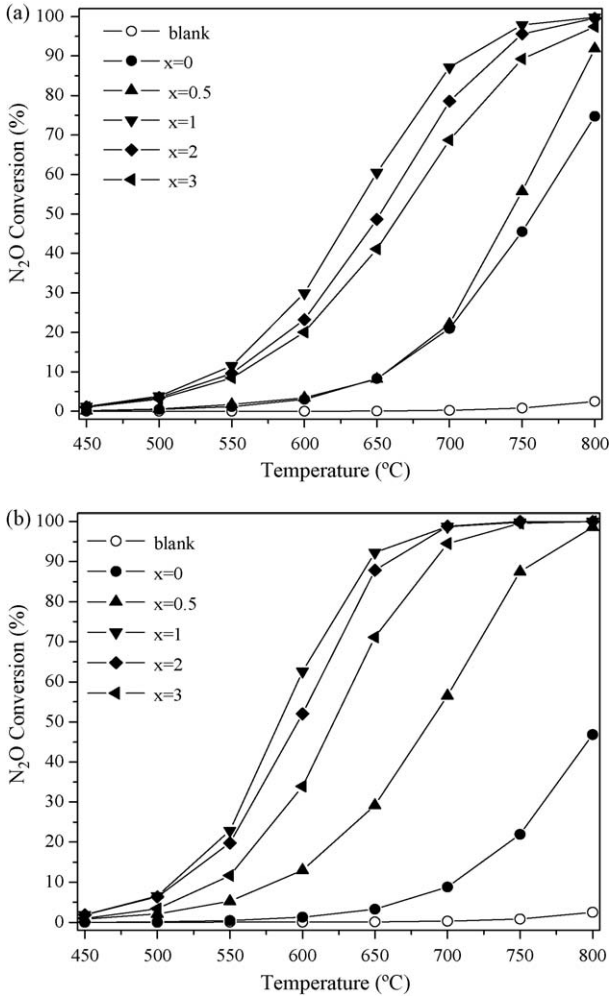

Fig. 7. Effect of Mn content on the catalytic performances of (a) $LaMn_xAl_{(12-x)}O_{19}$-1200 and (b) $BaMn_xAl_{(12-x)}O_{19}$-1200 catalysts.

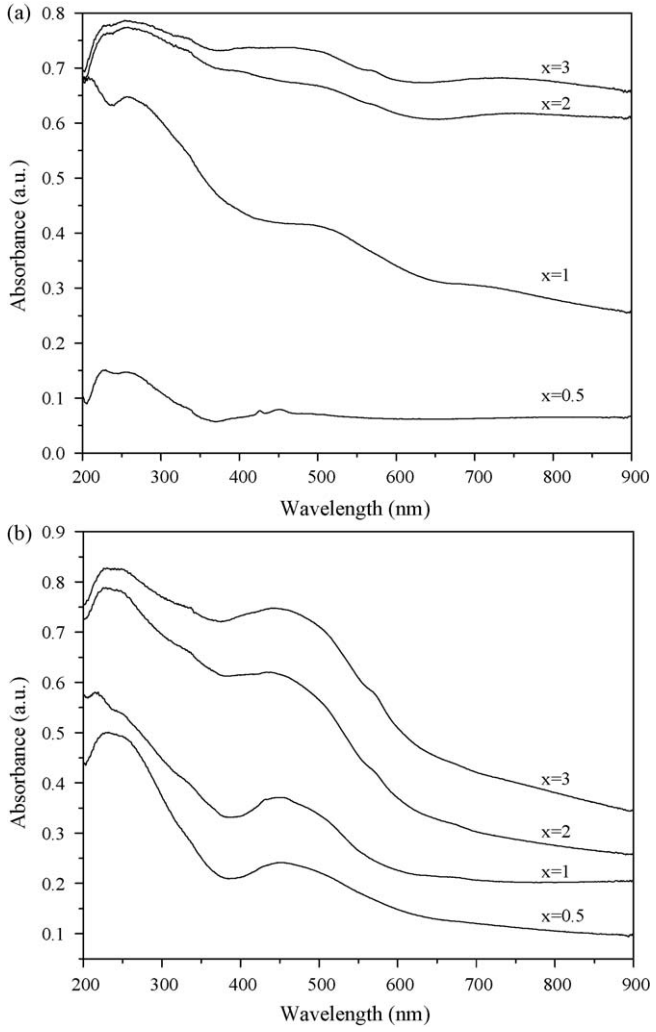

Fig. 8. UV–vis spectra of (a) $LaMn_xAl_{(12-x)}O_{19}$-1200 and (b) $BaMn_xAl_{(12-x)}O_{19}$-1200 catalysts.

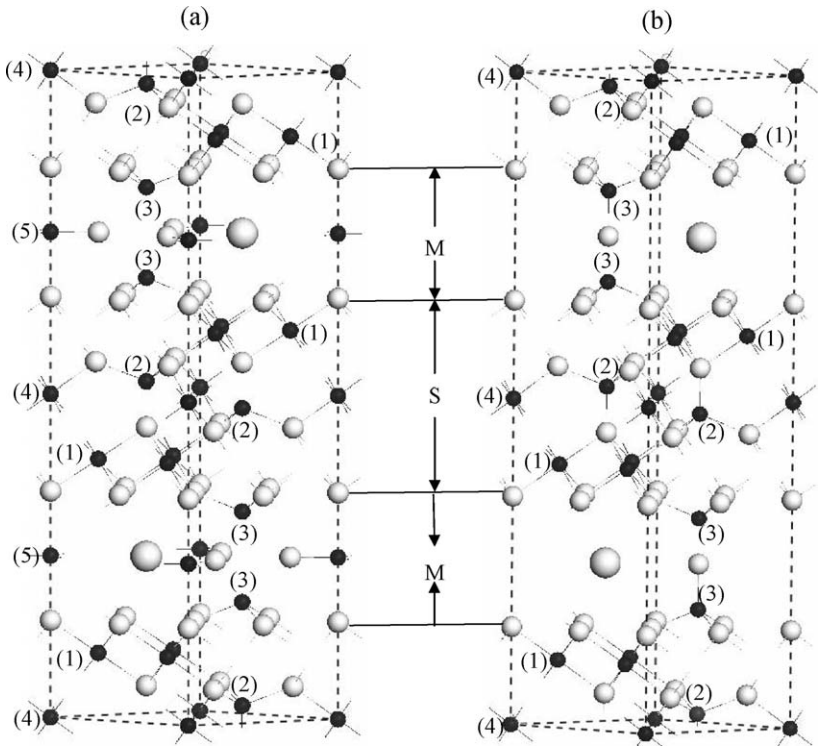

Fig. 9. The structure of hexaaluminate (M: mirror plane; S: spinel block) (a) MP structure; (b) β-Al_2O_3 structure. (●, La or Ba; ●, O; ●, Al).

Mn^{2+} (d^5) d–d transitions are both spin and orbitally forbidden [43]. Therefore, it is probable that both Mn^{2+} and Mn^{3+} are present in the $LaMn_xAl_{(12-x)}O_{19}$ catalyst when $x = 1$. With further increasing the Mn content ($x = 2, 3$), the absorption bands of Mn^{3+} become stronger. According to the XRD patterns of the $LaMn_xAl_{(12-x)}O_{19}$ at $x = 2$ and 3 (Fig. 6a), the intensified absorption bands should be contributed by the Mn^{3+} in the impurity $LaMnO_3$ phase.

Unlike the La-hexaaluminate catalysts, all the Ba-hexaaluminates present broad but strong absorption band centered at 450–470 nm which corresponds to the unique spin allowed d–d transition for d^4 electronic configuration in octahedral position [13,43]. This result strongly suggests that even at a low Mn content ($x = 0.5$), Mn^{3+} can still enter into the octahedral position of the Ba-hexaaluminate structure. Correlating with the much higher catalytic activity of the $BaMn_xAl_{(12-x)}O_{19}$ than that of the $LaMn_xAl_{(12-x)}O_{19}$ at x = 0.5, we can speculate that the Mn^{3+} in the octahedral structure is more active than the Mn^{2+} in the tetrahedral structure. The good activity of the Mn/Al_2O_3-500 also confirms that Mn^{3+} is the active site for N_2O decomposition. However, at a high Mn content ($x = 2, 3$) of the $BaMn_xAl_{(12-x)}O_{19}$ catalyst, the UV–vis spectra look like that of Mn_3O_4 [41], which is consistent with XRD results. Therefore, we can conclude that the large cations (La^{3+} or Ba^{2+}) mainly influence the number of octahedral Mn^{3+} sites which act as the active sites for N_2O decomposition. In the La-hexaaluminate with a MP structure (Fig. 9a), Mn preferentially enters tetrahedral Al(2) sites at a low Mn content ($x = 0.5$) as Mn^{2+}, which is inactive for N_2O decomposition. Increasing the Mn content results in the substitution of octahedral Al(1) sites with Mn^{3+}, thus leading to the enhancement of the activity. However, excess amount of Mn will deposit on the surface of the hexaaluminate by forming inactive $LaMnO_3$ species, instead of entering into the framework of hexaaluminate. In the case of Ba-hexaaluminate with a β-Al_2O_3 structure (Fig. 9b), however, Mn^{3+} can replace the octahedral Al(1) sites even at a low Mn content ($x = 0.5$), as a result, the catalytic activity of the Ba-hexaaluminate is much higher than that of the La-hexaaluminate.

3.3. Design of two-bed reactor for pure N_2O decomposition

Since the Mn-substituted Ba-hexaaluminate is more active than the La-hexaaluminate, we subsequently investigated the catalytic performance of the BMA-1200 as the back-bed catalyst in a thruster for the decomposition of pure N_2O propellant. The design of the two-bed thruster is illustrated in Fig. 1 where the front bed of the thruster was loaded with 30 wt%Ir/Al_2O_3 to ensure the start-up of the reaction at a relatively low temperature while the back bed was composed of thermally stable BMA-1200 catalyst. In the first operation, the catalyst bed was preheated to 450 °C in order to ignite the reaction. As shown in Fig. 10, the two-bed catalyst worked continuously for 500 s in the first run and the pressure in the thruster was increased rather rapidly to a constant value ($P_c = 0.25$ MPa) due to decomposition of N_2O. The two-bed catalyst was so active and thermally stable that the 500 s run could proceed successfully for 6 cycles. Moreover, the ignition temperature in the second 500 s run was decreased to 350 °C and further down to

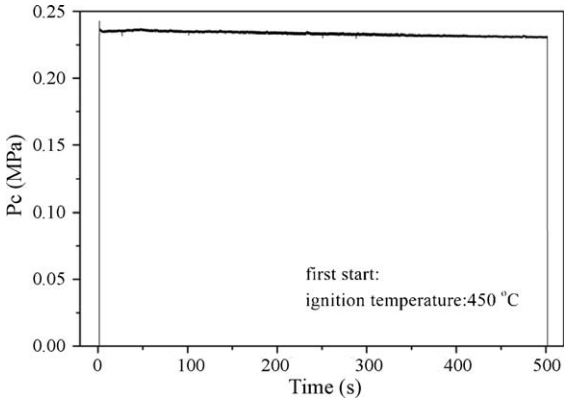

Fig. 10. Plot of the chamber pressure versus reaction time in the first 500 s run over the two-bed catalyst in a 0.1 N thruster.

250 °C in the following 4 runs (P_c profiles are not shown here), demonstrating the excellent ignition performance of this two-bed configuration. After the sixth reaction, the front-bed and back-bed catalysts were analyzed by XRF to determine if the active component was lost during the reaction. The results revealed that the Ir content in the front-bed catalyst was decreased from the original 30 wt% to 26.1 wt%. In contrast, the Mn content in the back-bed catalyst remained essentially the same as that of the fresh catalyst (6.9 wt% vs. 6.7 wt%). It should be stressed that the front-bed temperature was lower than the back-bed temperature. Even though, the Ir component in the front bed catalyst still had some loss. This result strongly demonstrates that the Mn-substituted Ba-hexaaluminate is a promising candidate as the back-bed catalyst for N_2O propellant decomposition.

4. Conclusion

In summary, we found that Mn-substituted hexaaluminates were active for high-concentration of N_2O decomposition. Large cations (Ba^{2+} and La^{3+}) greatly affected the catalytic performances by changing the number of octahedral Mn^{3+} sites entering into the framework of the hexaaluminates, which is regarded as the active sites for N_2O decomposition. The Ba-hexaaluminate with a β-Al_2O_3 structure has a larger fraction of octahedral Mn^{3+} than the La-hexaaluminate with a MP structure. As a result, the $BaMn_xAl_{(12-x)}O_{19}$-1200 exhibited much higher activity than the $LaMn_xAl_{(12-x)}O_{19}$-1200. The excellent high-temperature stability and good activity for N_2O decomposition make the Mn-substituted Ba-hexaaluminate a promising candidate as a back-bed catalyst for N_2O propellant decomposition.

Acknowledgments

Financial support was provided by the National Science Foundation of China (NSFC) grants (20773122, 20773124) and the External Cooperation Program of Chinese Academy of Sciences under grant (GJHZ200827).

References

[1] V. Zakirov, V. Goeman, T.J. Lawrence, M.N. Sweeting, in: Proceedings of the 14th Annual AIAA/USU Conference on Small Satellites, 21–24 August, USA, 2000.
[2] V. Zakirov, M. Sweeting, T. Lawrence, J. Sellers, Acta Astronautica 48 (2001) 353.
[3] S.A. Carabineiro, F.B. Fernandes, J.S. Vital, A.M. Ramos, I.M. Fonseca, Appl. Catal. B: Environ. 59 (2005) 181.
[4] H. Cheng, Y. Huang, A. Wang, L. Li, X. Wang, T. Zhang, Appl. Catal. B: Environ. 89 (2009) 391.
[5] E.V. Kondratenko, V.A. Kondratenko, M. Santiago, J. Pérez-Ramírez, J. Catal. 256 (2008) 248.
[6] P.J. Smeets, B.F. Sels, R.M. Teeffelen, H. Leeman, E.J.M. Hensen, R.A. Schoonheydt, J. Catal. 256 (2008) 183.
[7] F. Kapteijn, J. Rodriguez-Mirasol, J.A. Moulijn, Appl. Catal. B: Environ. 9 (1996) 25.
[8] A. Baylet, S. Royer, P. Marécot, J.M. Tatibouët, D. Duprez, Appl. Catal. B: Environ. 81 (2008) 88.
[9] E.E. Svensson, M. Boutonnet, S.G. Järås, Appl. Catal. B: Environ. 84 (2008) 241.
[10] R. Kikuchi, Y. Iwasa, T. Takeguchi, K. Eguchi, Appl. Catal. A: Gen. 281 (2005) 61.
[11] T. Utaka, S.A. Al-Drees, J. Ueda, Y. Iwasa, T. Takeguchi, R. Kikuchi, K. Eguchi, Appl. Catal. A: Gen. 247 (2003) 125.
[12] A. Baylet, S. Royer, C. Labrugère, H. Valencia, P. Marécot, J.M. Tatibouët, D. Duprez, Phys. Chem. Chem. Phys. 10 (2008) 5983.
[13] P. Artizzu-Duart, J.M. Millet, N. Guilhaume, E. Garbowski, M. Primet, Catal. Today 59 (2000) 163.
[14] S. Zhu, X. Wang, A. Wang, Y. Cong, T. Zhang, Chem. Commun. 17 (2007) 1695.
[15] S. Zhu, X. Wang, A. Wang, Y. Cong, T. Zhang, Catal. Today 131 (2008) 339.
[16] L. Ma, D.L. Trimm, Appl. Catal. A: Gen. 138 (1996) 265.
[17] J. Requies, M.C. Alvarez-Galvan, V.L. Barrio, P.L. Arias, J.F. Cambra, M.B. Güemez, A. Manrique Carrera, V.A. de Peña O'Shea, J.L.G. Fierro, Appl. Catal. B: Environ. 79 (2008) 122.
[18] L. Lietti, C. Cristiani, G. Groppi, P. Forzatti, Catal. Today 59 (2000) 191.
[19] G. Groppi, M. Bellotto, C. Cristiani, P. Forzatti, Pl. Villa, J. Mater. Sci. 34 (1999) 2609.
[20] M. Bellotto, G. Artioli, C. Cristiani, P. Forzatti, G. Groppi, J. Catal. 179 (1998) 597.
[21] M. Machida, A. Sato, M. Murakami, T. Kijima, H. Arai, J. Catal. 157 (1995) 713.
[22] M. Machida, A. Sato, T. Kijima, H. Inoue, K. Eguchi, H. Arai, Catal. Today 26 (1995) 239.
[23] A. Baylet, S. Royer, P. Marécot, J.M. Tatibouët, D. Duprez, Appl. Catal. B: Environ. 77 (2008) 237.
[24] B.W.-L. Jang, R.M. Nelson, J.J. Spivey, M. Ocal, R. Oukaci, G. Marcelin, Catal. Today 47 (1999) 103.
[25] M. Machida, K. Eguchi, H. Arai, J. Catal. 123 (1990) 477.
[26] F. Yin, S. Ji, P. Wu, F. Zhao, C. Li, J. Mol. Catal. A: Chem. 294 (2008) 27.
[27] G. Groppi, C. Cristiani, P. Forzatti, Appl. Catal. B: Environ. 35 (2001) 137.
[28] S. Li, X. Wang, J. Alloys Compd. 432 (2007) 333.
[29] J. Pérez-Ramírez, M. Santiago, Chem. Commun. 6 (2007) 619.
[30] M. Santiago, J. Pérez-Ramírez, Environ. Sci. Technol. 41 (2007) 1704.
[31] H. Tian, T. Zhang, X. Sun, D. Liang, L. Lin, Appl. Catal. A: Gen. 210 (2001) 55.
[32] J.R. Wallbank, P.A. Sermon, A.M. Baker, L. Courtney, R.M. Sambrook, European Space Agency, ESA SP 557, 2004, p. 125 (special publication).
[33] E.R. Stobbe, B.A. de Boer, J.W. Geus, Catal. Today 47 (1999) 161.
[34] G. Groppi, C. Cristiani, P. Forzatti, J. Catal. 168 (1997) 95.
[35] Y. Zhang, Q. Li, X. Ma, X. Cao, Mater. Lett. 62 (2008) 923.
[36] H. Arai, M. Machida, Appl. Catal. A: Gen. 138 (1996) 161.
[37] M.S. Yalfani, M. Santiago, J. Pérez-Ramírez, J. Mater. Chem. 17 (2007) 1222.
[38] S.I. Woo, S.K. Kang, J.M. Sohn, Appl. Catal. B: Environ. 18 (1998) 317.
[39] V. Zakirov, M. Sweeting, T. Lawrence, in: Proceedings of the 15th Annual AIAA/USU Conference on Small Satellites, 13–16 August, USA, 2001.
[40] J.G. Park, A.N. Cormack, J. Solid State Chem. 130 (1997) 199.
[41] F. Milella, J.M. Gallardo-Amores, M. Baldi, G. Busca, J. Mater. Chem. 8 (1998) 2525.
[42] F. Laville, D. Gourier, A.M. Lejus, D. Vivien, J. Solid State Chem. 49 (1983) 180.
[43] P. Artizzu-Duart, Y. Brullé, F. Gaillard, E. Garbowski, N. Guilhaume, M. Primet, Catal. Today 54 (1999) 181.